THE STRENGTH REDUCTION METHOD AS A TOOL FOR SLOPE STABILITY ASSESSMENT

CORINA-MARIA ILADIE[1], ZHAO QI[2], MARIAN-GABRIEL BORDEIANU[3], FLORIN DUMITRU POPESCU[4], ANDREI ANDRAŞ[5]

Abstract: The strength reduction method, combined with finite element analysis, is a widely used technique for determining the factor of safety (FOS) in geomechanics, particularly in assessing the stability of slopes and embankments. This method involves progressively reducing the material properties of the soil until failure occurs. While the definition of the factor of safety can vary in other contexts, in geotechnical engineering, it is specifically defined in terms of the soil's strength parameters.

The strength reduction method is particularly suited to linear failure criteria, such as the Mohr–Coulomb criterion. When applied using this criterion, the cohesion, internal friction angle, and dilatation angle of the soil are simultaneously reduced until the system loses mechanical equilibrium. This gradual reduction weakens the soil's shear strength, ultimately leading to instability. Such instability manifests as the collapse of the slope under a specific combination of loads, material properties, and boundary conditions. The factor of safety (FOS) is calculated as the ratio of the soil's initial cohesion to the cohesion at the point of failure.

Keywords: slope stability, factor of safety, finite elements, strength reduction method.

1. THEORETICAL BACKGROUND

Generally, the Mohr–Coulomb yield function F is expressed as:

$$F = m\sqrt{J_2} + \frac{\sin\Phi}{3} I_1 - C\cos\Phi \tag{1}$$

and the plastic potential Q is expressed by the equations:

[1] *Ph.D. student Eng., University of Petroşani, iladie.corina@yahoo.com*
[2] *Ph.D. student Eng., University of Petroşani, zhaoqi0715@hotmail.com*
[3] *Ph.D. student Eng., University of Petroşani, gabriel.bordeianu@gmail.com*
[4] *Prof. Ph.D. Eng., University of Petroşani, fpopescu@gmail.com*
[5] *Prof. Ph.D. Eng., University of Petroşani, andrei.andras@gmail.com*

$$Q = m_q \sqrt{J_2} + \frac{\sin \Psi}{3} I_1 - C \cos \Psi \tag{2}$$

where I_1 represents the first stress invariant and J_2 the second deviatoric stress invariant. The parameterized angle of internal friction Φ, the parameterized dilatation angle Φ, and the parametrized cohesion C are written as:

$$C = \frac{c}{\mathrm{FOS}}, \quad \Phi = \arctan\left(\frac{\tan \phi}{\mathrm{FOS}}\right), \quad \Psi = \left(\frac{\tan \psi}{\mathrm{FOS}}\right) \tag{3}$$

Here, c represents cohesion, ϕ is the angle of internal friction, and ψ is the dilatation angle. It is important to note that c, ϕ, and ψ are the unreduced initial parameters of material. Under the associative flow rule, $\psi = \phi$.

For the non-associative flow rule, ψ remains constant as long as it is less than ϕ. Nevertheless, in our example, ψ is set to zero for the non-associative flow rule. As a result, no special adjustments are required, and (3) applies to both the associative and non-associative flow rules.

It is worth noting that using the strength reduction method with the non-associative flow rule can lead to numerical instabilities, potentially causing a non-unique failure surface and factor of safety (FOS). To address this, the associative flow rule is applied using reduced values of the angle of internal friction and cohesion, to approximate the behavior of the non-associative flow rule. The reduced angle of internal friction ϕ' and reduced cohesion c' are expressed as:

$$c' = \beta, \quad \phi' = \arctan\left(\beta \cdot \tan \phi\right) \tag{4}$$

Here, the factor of reduction β can be expressed as:

$$\beta = \frac{\cos\left(\arctan\left(\frac{\tan \phi}{\mathrm{FOS}}\right)\right)\cos\left(\arctan\left(\frac{\tan \psi}{\mathrm{FOS}}\right)\right)}{1 - \sin\left(\arctan\left(\frac{\tan \phi}{\mathrm{FOS}}\right)\right)\sin\left(\arctan\left(\frac{\tan \psi}{\mathrm{FOS}}\right)\right)} \tag{5}$$

Consequently, (3) is rewritten using the reduced cohesion c' and the reduced angle of internal friction ϕ', for both the associative and the non-associative flow rules, as the factor of reduction β is unitary for the associative flow rule.

2. THE DEFINITION OF THE MODEL

The cross section of the soil embankment used for the simulation is shown in Figure 1. The dimensions L_1 and L_2 are lengths of 85 m and 20 m, respectively, and the dimensions H_1 and H_2 are heights of the embankment of 20 m and 10 m, respectively. The slope angle α is variable from 15° to 45°.

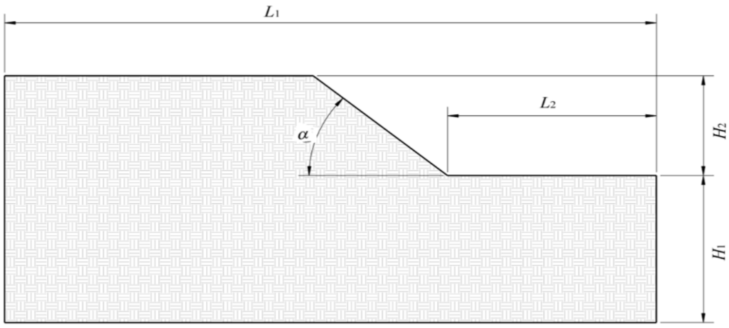

Fig.1. Cross section and dimensions of the slope

The material properties for both the associative and the non-associative plasticity models, are summarized in Table 1.

Table 1 **Material properties**

Property	Material 1	Material 2
E	20 MPa	20 MPa
υ	0.3	0.3
c	20 kPa	20 kPa
φ	25°	25°
ψ	0°	25°
ρ	1940 kg/m^3	1940 kg/m^3

The modeling and simulation were carried out in the COMSOL Multiphysics software for a 2D model using the `Structural Mechanics → Solid Mechanics (solid)` module. Figure 2 presents the material parameters of the dump in the format in which they were entered into the COMSOL software.

Name	Expression	Value	Description
E_soil	20[MPa]	2E7 Pa	Modulul Young
nu_soil	0.3	0.3	Coeficientul Poisson
rho_soil	19[kN/m^3]/g_const	1937.5 kg/m³	Densitatea Solului
c	20[kPa]	20000 Pa	Coeziunea
phi	25[deg]	0.43633 rad	Unghiul de Frecare
psi	0[deg]	0 rad	Unghiul de Dilatare

Fig.2. Characteristic Parameters of the Dump Materia

Similarly, the characteristic values of the dump material parameters were implemented for the two cases considered: associative plasticity and non-associative plasticity. The difference between the two cases lies in the value of the parameter ψ, which is set to 0 and 25 degrees, respectively.

In the `Definition` section, the calculation relationships corresponding to the variables used in the simulation were implemented, as shown in Figure 3.

Name	Expression	Unit	Description
beta_f	cos(atan(tan(phi)/FOS))*cos(atan(tan(psi)/FOS))/(1-sin(atan(tan(phi)/FOS))*sin(atan(tan(psi)/FOS)))		Factorul de reducere
c_r	beta_f*c	Pa	Reducerea coeziunii
phi_r	atan(beta_f*tan(phi))	rad	Reducerea unghiului de frecare
c_p	c_r/FOS	Pa	Coeziunea parametrizată
phi_p	atan(tan(phi_r)/FOS)	rad	Unghiul de frecare parametrizat

Fig.3. Defining Simulation Variables

The variables defining the material properties are presented in Table 2.

Table 2 **Variables Corresponding to Material Properties**

Property	Variable	Expresion	Unit
Young's modulus	`E`	`E_soil`	Pa
Poisson's ratio	`nu`	`nu_soil`	1
Density	`rho`	`rho_soil`	kg/m3
Cohesion	`cohesion`	`c_p`	Pa
Angle of internal friction	`internalphi`	`phi_p`	rad

The finite element mesh geometry of the model is shown in Figure 4. For the entire simulation domain, the `Finer` option was selected for the finite element size, while the `Extremely Fine` option was chosen for the refinement region. The geometric shape of the finite elements is triangular.

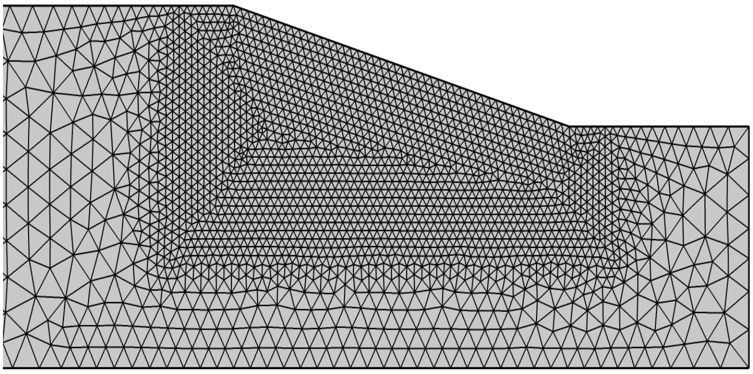

Fig.4. The finite elements mesh geometry

3. RESULTS

Following the calculations, the factor of safety (FOS) was initially determined for different slope angles, as shown in Figure 5. The FOS decreases as the slope angle increases, which is expected.

Additionally, the FOS for the same slope inclination with non-associative plasticity (Material 1) is always lower than with associative plasticity (Material 2).

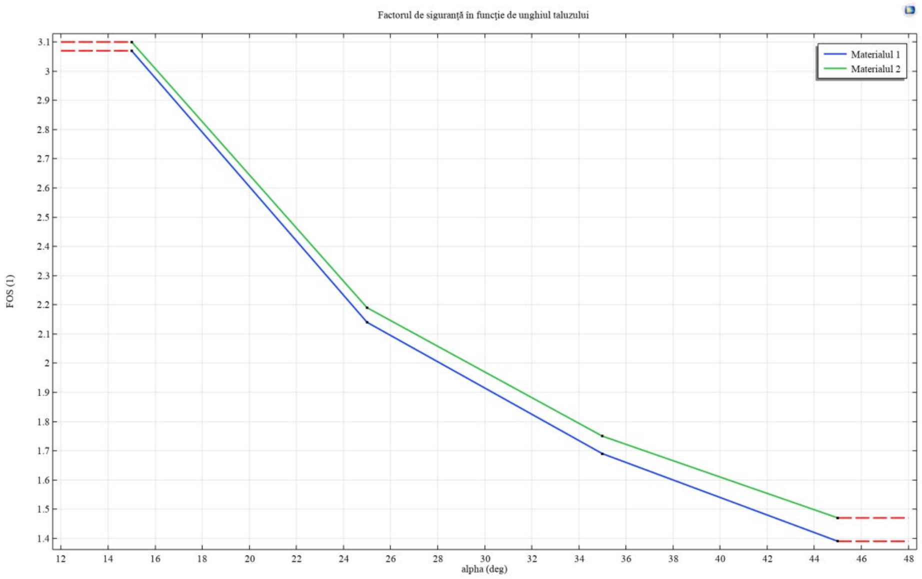

Fig. 5. Factor of safety as function of slope angle

It can also be observed that the influence of considering non-associative plasticity is marginal for the selected material parameters. The equivalent plastic deformation for different slope angles just before failure is shown in Figures 6 and 7 for the two materials considered. The localization of plastic deformation zones in Figures 6 and 7 provides an indication of the failure surface for various slope angles. It is evident that for smaller slope angles, multiple failure surfaces develop within the sloped mass.

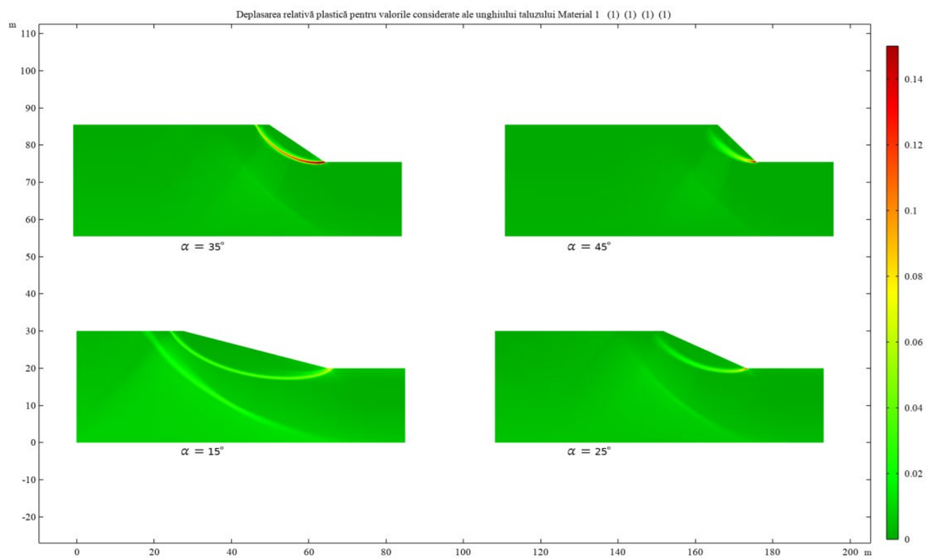

Fig. 6. Relative Plastic Displacement as a Function of Slope Angle, Material 1

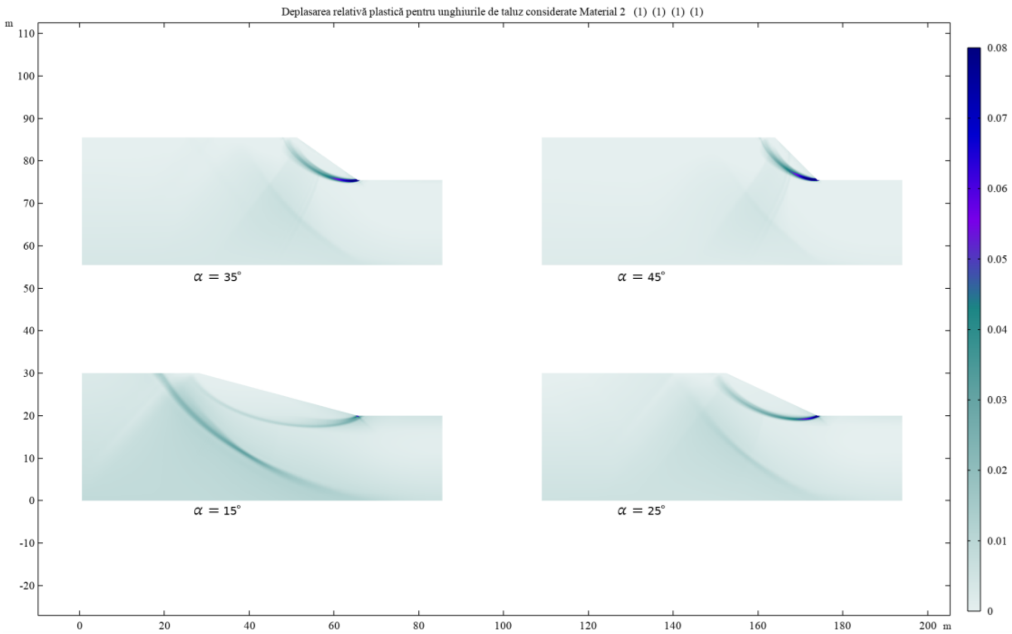

Fig. 7. Relative Plastic Displacement as a Function of Slope Angle, Material 2

Figure 8 illustrates the 2D cross-sectional displacements of the slope corresponding to Material 1 for the four slope inclination angles considered.

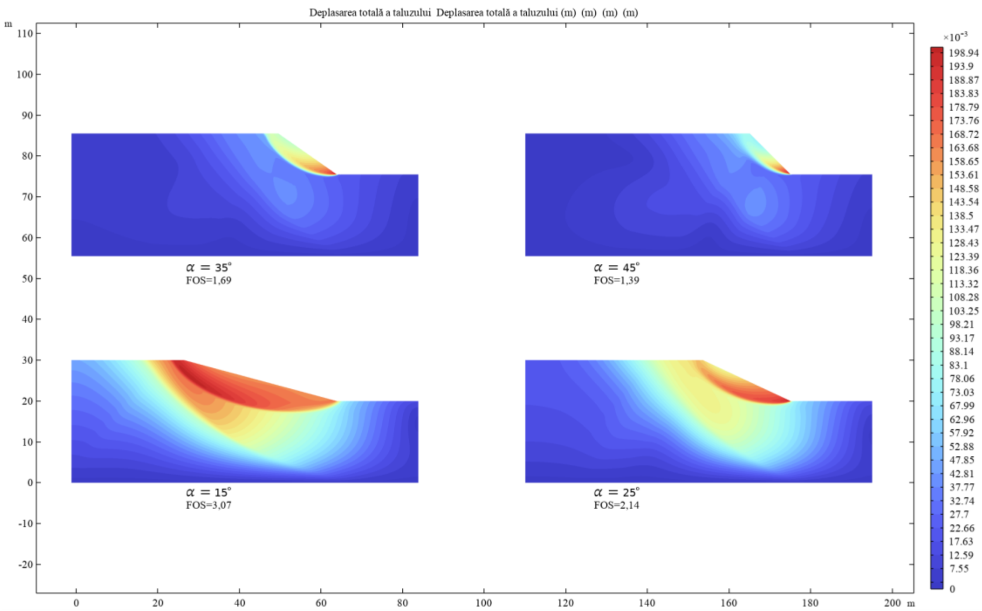

Fig. 8. Slope Displacements for Material 1

Figure 9 shows the displacement magnitude for Material 2 at a slope inclination angle of 45º and a stability factor FOS of 1.39.

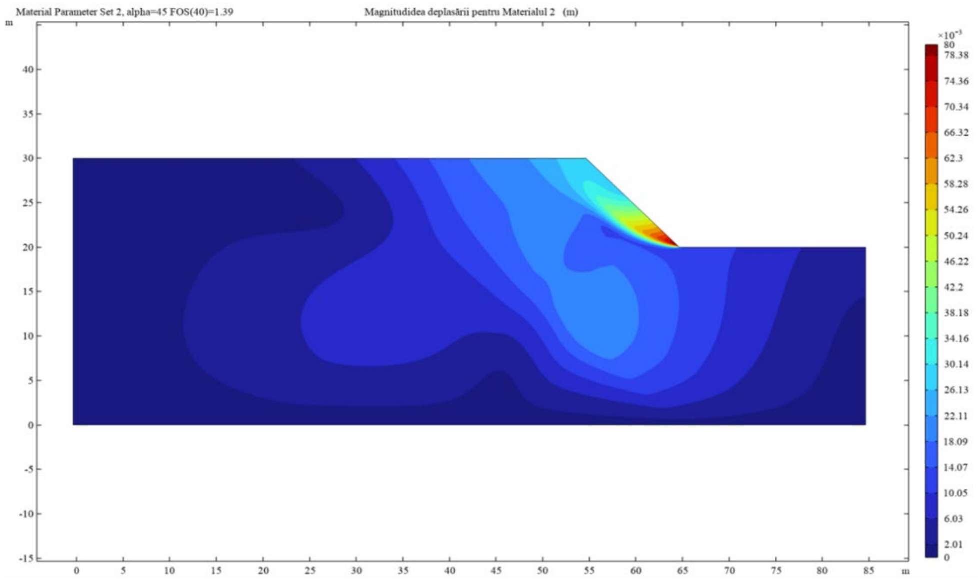

Fig. 9. Displacement Magnitude for Material 2 at 45º

CONCLUSIONS

This study conducted a stability analysis for a hypothetical slope through numerical simulation, representative in terms of geometry, dimensions, and material characteristics of dumps (dump steps) in the Motru Basin.

The theoretical aspects of the strength reduction method were presented, which, in combination with the finite element method, proved to be a valuable tool for addressing geotechnical problems. Recently, there have been efforts to apply this method to slope stability analysis. For this study, COMSOL was chosen as the software tool, a computational package well-suited for solving slope stability problems. It includes modules for implementing geometric models, material properties, failure (yield) hypotheses, and the necessary calculation algorithms for applying the strength reduction method.

Quantitative results included the factor of safety (FOS) values for various slope angles. As expected, the FOS decreases as the slope angle increases. Additionally, the FOS value for the same slope angle in the non-associative plasticity case (Material 1) is consistently lower than in the associative plasticity case (Material 2). This finding indicates that the influence of non-associative plasticity is marginal for the chosen material parameter values.

It was also observed that multiple failure surfaces develop within the sloped mass, a phenomenon more pronounced at lower slope angles.

The ability to visualize displacement magnitudes, not just relative deformations, across the entire analyzed mass enables a better estimation of the rock mass behavior based on inclination. This visualization helps correlate qualitative aspects of displacements and deformations with quantitative results, such as the factor of safety (FOS), providing more comprehensive information for stability assessment.

Additionally, the capability to visualize not only the magnitude of displacements but also the direction and sense of movement at different points within the analyzed area is particularly useful for predicting the future behavior of the slope.

The stability analysis method and the computational tool used for its implementation represent a significant step forward in refining methods for assessing geotechnical risk. This is particularly relevant for anthropogenic landscape modifications caused by open-pit lignite mining, which remains the most significant and lasting environmental impact of such operations.

REFERENCES

[1]. **Andraș, A., Brînaș, I., Radu, S.M., Popescu, F.D., Popescu, V., Budilică, D.I.** *Investigation of the Thermal Behaviour for the Disc-Pad Assembly of a Mine Hoist Brake Using COMSOL Multiphysics.* Acta Tech. Napoc.-Ser. Appl. Math. Mech. Eng. 64, 227–234, 2021.

[2]. **Popescu, F. D., Radu, S. M., Kotwica, K., Andraș, A., Kertesz, I.** *Simulation of the time response of the ERc 1400-30/7 bucket wheel excavator's boom during the excavation process.* Sustainability, 11(16), 4357, 2019.

[3]. **Popescu, F.D., Radu, S.M., Andras, A., Brinas, I.K.** *A grafo-numeric method of determination of the operation power of the rotor of EsRc-1400 bucket wheel excavator using computer simulation in SolidWorks.* MATEC Web Conf. 290, 04007, 2019.

[4]. **Popescu, F. D., Radu, S. M., Andras, A., Kertesz (Brînaș), I.** *Simulation of the frequency response of the ERC 1400 Bucket Wheel Excavator boom, during the excavation process*, New Trends in Production Engineering, Vol. 2, Issue 1, pp. 153-167, 2019.

[5]. **Radu, S.M., Popescu, F.D., Andras, A., Kertesz, I.**, *Transport si instalaţii miniere*, Editura Universitas, Petroşani, 2018, ISBN 978-973-741-587-5

[6]. **Nan MS, Kovacs J., Popescu FD**. *Balance control by weighing and tensiometric measurements of bucket wheel excavators*, "WSEAS Transactions On Systems And Control" 2008, 11, 3: 927–936.